

Active restructuring of cytoskeleton composites leads to increased mechanical stiffness, memory, and heterogeneity

Janet Y. Sheung^{1*}, Daisy H. Achiriloae¹, Karthik Peddireddy², Gloria Lee², Michael J. Rust³, Moumita Das⁴, Jennifer L. Ross⁵, Rae M. Robertson-Anderson^{2*}

¹W. M. Keck Science Department, Scripps College, Pitzer College, and Claremont McKenna College, 925 N. Mills Ave. Claremont CA 91711, USA

²Department of Physics and Biophysics, University of San Diego, 5998 Alcala Park, San Diego, CA, 92110, USA

³Department of Molecular Genetics and Cell Biology, University of Chicago, Chicago, IL 60637, USA.

⁴ School of Physics and Astronomy, Rochester Institute of Technology, Rochester, NY 14623, USA.

⁵Department of Physics, Syracuse University, Syracuse, NY 13244, USA.

ABSTRACT

The composite cytoskeleton, comprising interacting networks of semiflexible actin and rigid microtubules, actively generates forces and restructures using motor proteins such as myosins to enable key mechanical processes including cell motility and mitosis. Yet, how motor-driven activity alters the mechanics of cytoskeleton composites remains an open challenge. Here, we perform optical tweezers microrheology on actin-microtubule composites driven by myosin II motors to show that motor activity increases the linear viscoelasticity and elastic storage of the composite by active restructuring to a network of tightly-packed filament clusters and bundles. Our nonlinear microrheology measurements performed hours after cessation of activity show that the motor-contracted structure is stable and robust to nonlinear forcing. Unique features of the nonlinear response include increased mechanical stiffness, memory and heterogeneity, coupled with suppressed filament bending following motor-driven restructuring. Our results shed important new light onto the interplay between viscoelasticity and non-equilibrium dynamics in active polymer composites such as the cytoskeleton.

The cytoskeleton is an active composite of protein filaments capable of restructuring on demand to meet the wide variety of mechanical properties needed by eukaryotic cells, such as structural rigidity to counter external pressure, malleability to navigate narrow openings, and shape change required in mitosis.¹ Two key biopolymers, semiflexible actin filaments and rigid microtubules, contribute to this versatility by forming interacting viscoelastic networks.² In addition, molecular motors, such as actin-associated myosins, stochastically bind to and actively pull on filaments, generating forces to contract and rearrange the cytoskeleton.^{3,4} Motor-driven active dynamics play a critical role in enabling the cytoskeleton to quickly tune its mechanical properties to achieve a myriad of different functions in response to environmental cues. At the same time, there is mounting evidence that interactions between actin filaments and microtubules play equally important roles in mechanical processes such as mitosis and crawling.¹ As such, the cytoskeleton is an exemplar of active matter that has been intensely studied not only for its biological relevance but for its importance in the design of active non-equilibrium materials.^{5,6} Nevertheless, the mechanical properties of the active composite cytoskeleton, critical to biological and materials applications, remain poorly understood.

Numerous *in vitro* studies have been carried out on actomyosin systems, reporting a range of structural properties and dynamics depending on the concentrations of actin, myosin and passive crosslinkers.^{7–16} With sufficiently high crosslinker concentration, actomyosin activity induces large-scale contraction and coarsening of disordered actin networks.¹³ However, below this critical crosslinker density, networks undergo destabilizing flow and rupturing into disconnected foci, thereby weakening the network.^{17–20} We previously showed that incorporating microtubules into an actomyosin network provides a mechanical scaffold with which the actin network entangles, and which enables controlled contractile dynamics, without flow or rupturing, in the absence of crosslinkers²⁰. We also showed that the controlled contraction of both actin and microtubule networks was highly uniform and ballistic with a contraction speed of $v \approx 11.3$ nm/s, ~7x slower than actomyosin systems without microtubules.

The rheological properties of actomyosin systems are far less well-understood, primarily due to the fact that the microrheology methods typically used to investigate similar biological systems rely on the generalized Stokes Einstein relation (GSER) to derive viscoelastic moduli from the thermal fluctuations of embedded particles.²¹ In non-equilibrium active systems, GSER is violated over frequency ranges comparable to those of the motor-driven activity.²² Previous attempts to investigate the mechanics of actomyosin systems have shown that particle fluctuations are dominated by motor activity at low frequencies while thermal fluctuations dominate the high-frequency regime.²³ However, how interactions between actin and microtubules impact the rheological properties of actomyosin systems remains completely unexplored.

Here, we perform linear and nonlinear optical tweezers microrheology to characterize the microscale force response of photo-activated myosin-driven actin-microtubule composites before, during and following myosin activity (Fig 1, SI Methods). We circumvent GSER violation by performing measurements on a judiciously tuned active composite which visibly restructures on the order of minutes, yet is still slow enough ($\omega_{active} < 0.1$ rad/s) to be considered quasi-static (i.e., dominated by thermal fluctuations) for frequencies above ~ 1 rad/s. Further, with the use of the light-sensitive myosin inhibitor, blebbistatin, we precisely control the location and duration of motor activity to enable measurements to be performed before, during and after motor activity in different regions of the same sample. We also perform nonlinear straining measurements before and after activity to characterize how motor-driven restructuring alters the nonlinear force response, stiffness and relaxation dynamics of the composite. We couple our measurements with fluorescence imaging of the composite before and after measurements to show that the increased elasticity, stiffness, mechanical heterogeneity, and mechano-memory is a result of mesoscale restructuring from a homogeneous entangled mesh to a more sparsely connected network of contracted clusters and bundles.

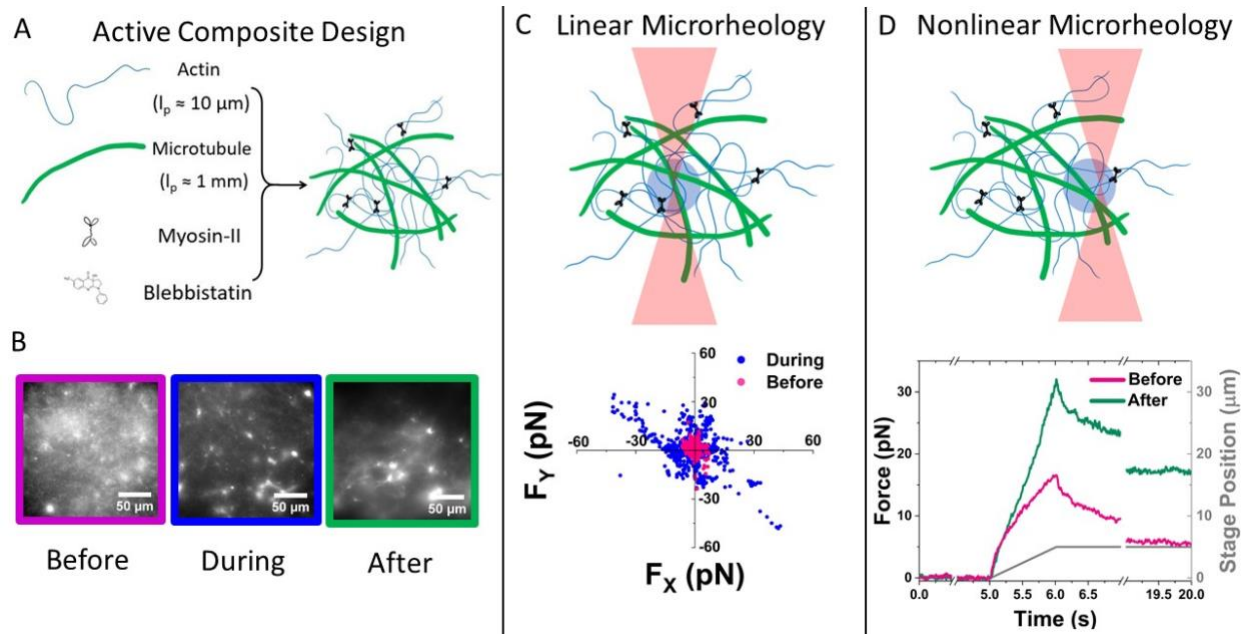


Figure 1. Optical tweezers microrheology characterizes how actomyosin activity alters the mechanical response of actin-microtubule composites. (A) Cartoon of composite comprised of semiflexible actin filaments (2.9 μM), rigid microtubules (2.9 μM), and actin-associated myosin II minifilaments (0.24 μM), prepared as described in SI. Blebbistatin allows for myosin II motors to be selectively photo-activated by 488 nm illumination. (B) 1064x1064 pixel fluorescence images of actin filaments in the composite (10% of actin monomers are labeled with AlexaFuor568), acquired before (magenta), during (blue), and 2 hrs after (green) myosin II activity. (C) Linear Microrheology. (Top) Schematic of measurement in which we optically trap a 4.5- μm diameter microsphere and track its force fluctuations in x- and y- directions (F_x, F_y) for 3 mins. (Bottom) Scatter plot of detected forces from all trials, before (magenta) and during (blue) activity, at all timepoints. (D) Nonlinear Microrheology. (Top) Schematic of measurement in which we displace an optically trapped microsphere 5 μm through the composite at a constant speed of 5 $\mu\text{m}/\text{s}$. We measure the force exerted on the microsphere before, during and following the displacement to determine the nonlinear force response and subsequent relaxation dynamics. Example force measurement, before (magenta) and after (green) motor activity. The gray curve shows the position of the piezoelectric stage that displaces the bead relative to the composite.

To characterize the linear force response, we measure the force fluctuations of optically trapped beads within the composite before and during myosin activity (Fig 1C). x - and y - components of the measured force (F_x, F_y) show significant increases in the magnitude and variance of force fluctuations during myosin activity in all directions in the detection plane (Fig 2A). The radial force magnitude $F_R = (F_x^2 + F_y^2)^{1/2}$ over time similarly shows a sustained increase in force, as well as increased heterogeneity, during motor activity (Fig 2B). Further, in some cases,

the force that the active composite exerted on the trapped bead during activity increased beyond the strength of the trap and the bead was lost before the end of the 360 s trial, as shown in Fig 2B.

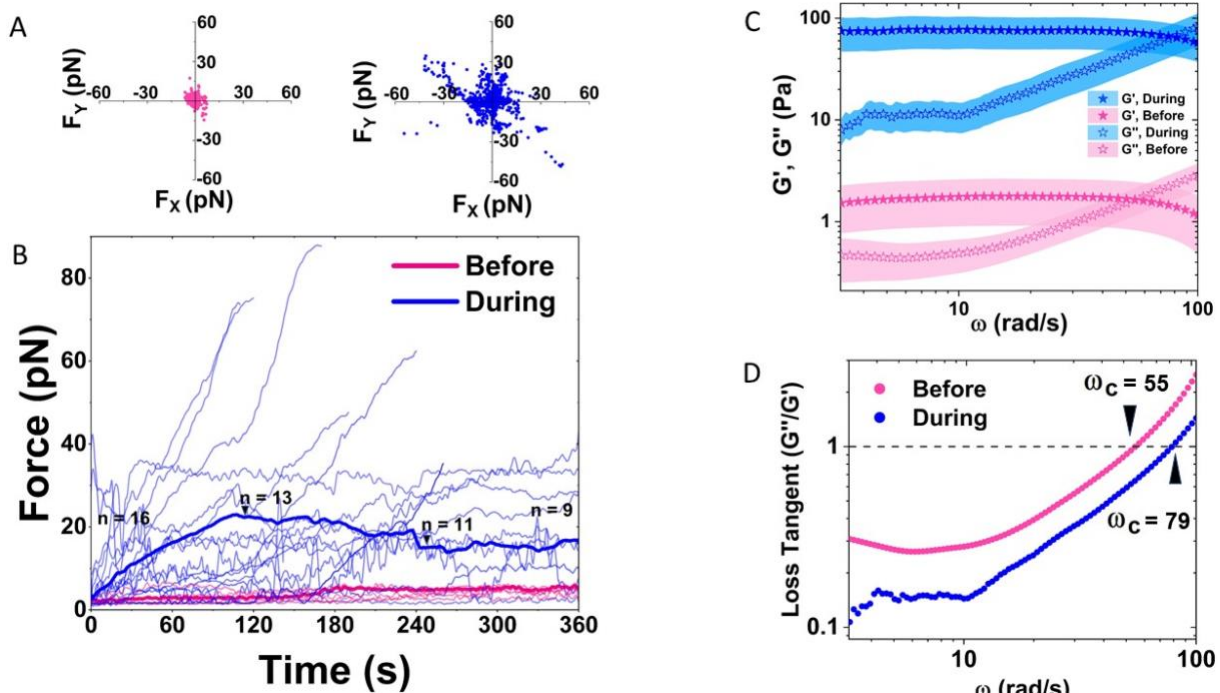


Figure 2. Myosin-driven activity increases the viscoelastic moduli and mechanical memory of actin-microtubule composites. (A) x and y components of the forces exerted on optically trapped microspheres embedded in myosin-driven actin-microtubule composites before myosin activation (magenta, left) and during 3 minutes of myosin activity (blue, right). Data shown is for all time points during each of the trials. (B) Radial force magnitude $F_R = (F_x^2 + F_y^2)^{1/2}$ versus time before (magenta) and during (blue) motor activity. Thin lines indicate individual trials and thicker lines indicate average over all trials. The force generated by the motors during activity exceeded the strength of the optical tweezers for some trials, leading to the truncated force curves shown. Arrows above the average force curve during activity indicate locations where the number of individual trials contributing to the average decreases due to truncated trials. (C) Frequency-dependent elastic ($G'(\omega)$, filled symbols) and viscous ($G''(\omega)$, open symbols) moduli before (magenta) and during (blue) activity. The shaded region surrounding each data curve indicates standard error. (D) Loss tangent ($\tan \delta = G''/G'$) versus frequency derived from the data shown in (C). Myosin activity decreases $\tan \delta$ across all frequencies and increases the crossover frequency ω_c .

To determine the role that this apparent motor-driven restructuring has on the viscoelastic properties of the composites we determine the frequency-dependent storage and loss moduli, $G'(\omega)$ and $G''(\omega)$, from our measured forces using GSER as previously described (SI Methods, Fig 2C).²³⁻²⁵ Because GSER is only strictly valid for steady-state thermal systems, we restrict our analyses to frequencies well above the frequency of the active motor driving ω_{active} . To determine this frequency, we use our previously measured contraction velocity of $v \approx 11.3$ nm/s for actin and microtubules in the myosin-driven composite studied here.²⁰ From this speed we compute an effective frequency $\omega_{active} = 2\pi\dot{\gamma}_{active} \approx 0.06$ rad/s for the strain exerted on a trapped bead of radius R by the motor-driven composite during motor-driven contraction via $\dot{\gamma} = 3v/\sqrt{2}R$.²⁵ We can therefore safely approximate that our system is in quasi-steady-state for $\omega > 1$ rad/s (an order of magnitude higher than ω_{active}).

Both before and during motor activity, the viscoelastic moduli show strong elastic behavior with the storage modulus $G'(\omega)$, a measure of the elastic storage in the system, exhibiting an elastic plateau across the entire frequency regime, and $G'(\omega)$ exceeding $G''(\omega)$, the dissipative component of the response, for all but the highest frequencies (Fig 2C). With motor activity, both moduli increase over all measured frequencies by nearly two orders of magnitude, signifying substantial coarsening and increasing entanglement density, likely due to motor-driven contraction. Further, the increase in $G'(\omega)$, is larger than that for $G''(\omega)$, which we quantify by computing the loss tangent, $\tan \delta = G''/G'$, which is a measure of the relative dissipation in the system. As shown (Fig 2D), motor activity decreases $\tan \delta$, with the frequency-averaged value dropping ~38% from 0.62 before activity to 0.38, indicating an increase in the mechanical memory (i.e. elastic storage) of the composite.^{26,27}

From our measured moduli we also compute the crossover frequency, ω_c , at which $G'(\omega) > G''(\omega)$ and $\tan \delta > 1$. For entangled polymer systems this crossover frequency is a

measure of the entanglement time τ_e , i.e. the time at which filament-filament interactions become important.²⁸ We find ω_c increases from 55 rad/s to 79 rad/s with activation, corresponding to a decrease in τ_e from ~ 0.11 s to 0.08 s, similar to the previously measured value of ~ 0.06 s for inactive crosslinked actin-microtubule composites.²⁹ We can understand this decrease in τ_e as arising from the amplified filament-filament interactions that myosin motors, which stochastically bind neighboring filaments, enable, leading to a delayed crossover to rubbery flow.

To determine the extent to which the signatures of coarsening and contraction we observe during motor activity are preserved in the nonlinear regime, in which the composite is driven far from equilibrium, we perform nonlinear constant rate strain measurements. Specifically, we displace an optically trapped bead a distance of 5 μm at a constant speed of 5 $\mu\text{m/s}$ and measure the force during and after the strain to determine the nonlinear force response of the composite and the subsequent relaxation of imposed stress (Fig 1D). To separate the effects of motor-driven strain from the externally applied strain, we perform measurements two hours after we have ceased light-activation of the motors. Visual examination of the composite at this point shows no visible restructuring or athermal motion.

As shown in Fig 3A, the force response both before and after activity is solid-like over the entire strain, as evidenced by the linear dependence on strain, suggestive of strong network connectivity that is not easily disrupted by nonlinear forcing. However, the magnitude and slope of the force response after activity is substantially higher than before activity. To quantify the increased slope, which is a measure of the network stiffness, we compute the average differential modulus $K = dF/dx$ for each individual trial (Fig 3A inset). As shown, both the magnitude and spread of stiffness values increases following activity. The distribution in measured force curves likewise increases. These results suggest that motor-driven restructuring leads to a more heterogeneous network comprised, in part, by more tightly connected or bundled filaments that are stiffer and more readily resist imposed strain.

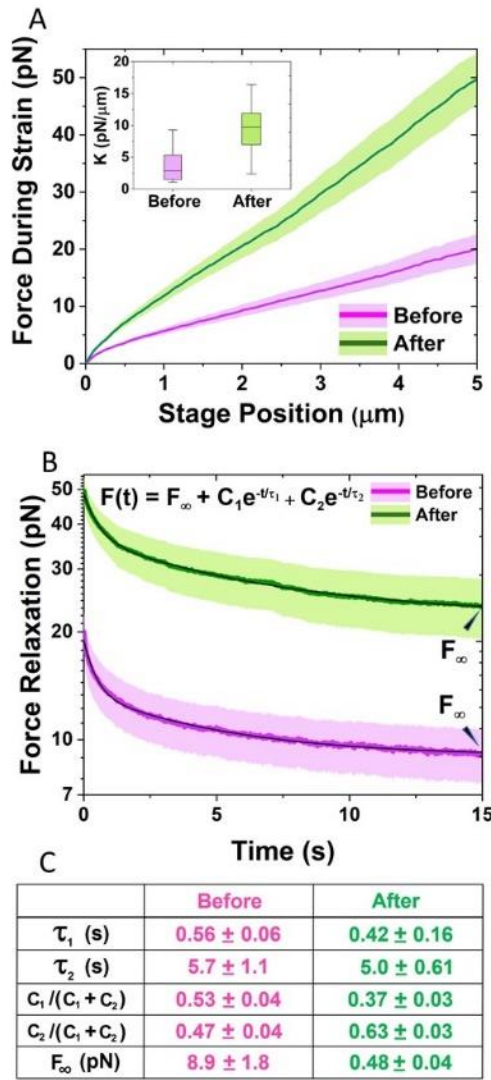


Figure 3. Myosin-driven restructuring increases the nonlinear force response, stiffness and heterogeneity of actin-microtubule composites. (A) Average force $F(x)$ exerted on the bead during nonlinear strain, measured before (magenta) and after (green) myosin activity. Shaded regions along each curve indicate standard error across all trials. Inset: Boxplot of differential modulus, $K = dF/dx$, found as the slope of $F(x)$ after $x=1$ μm for each trial. (B) Relaxation of force as a function of time following the strain, measured before (magenta) and after (green) motor activity. Both relaxation curves are well-fit to a sum of two exponentials with well-separated time constants and a non-zero offset: $F(t) = F_\infty + C_1 e^{-t/\tau_1} + C_2 e^{-t/\tau_2}$. (C) Table of fitting parameters from data shown in (B). The time constants, τ_1 and τ_2 , quantify the fast and slow relaxation timescales while $C_1/(C_1 + C_2)$ and $C_2/(C_1 + C_2)$ indicate the relative contribution of each relaxation mode to the force relaxation. F_∞ corresponds to the force that is sustained undissipated at the end of the relaxation period.

We next evaluate the relaxation of the imposed stress following strain (Fig 3B,C). Specifically, after the 5 μm strain, we hold the bead fixed for 15 seconds and measure the force decay as a function of time. Both before and after activity, composites relax a fraction of the imposed stress but maintain some degree of strain memory (i.e. non-zero force) at the end of the relaxation phase. However, this non-zero terminal force F_∞ , a signature of solid-like mechanics, is $\sim 3x$ higher following myosin-driven restructuring, in line with the increased stiffness and force response we measure during strain. Taking into account this non-zero terminal force, we find that both relaxation curves fit well to a sum of two exponentials with well-separated time constants: $F(t) = F_\infty + C_1 e^{-t/\tau_1} + C_2 e^{-t/\tau_2}$. We can interpret each decay as arising from a distinct relaxation mechanism with a characteristic decay time τ_i and a relative contribution to the overall relaxation $C_i/(C_1 + C_2)$.

To understand our fast relaxation timescale, τ_1 , we evaluate the predicted timescale for actin bending, $\tau_B \approx \gamma L / (\kappa (3\pi/2)^4)$ where $L \approx 8.7 \mu\text{m}$ is the actin filament length,³¹ $\kappa \approx l_p k_b T$ the bending rigidity, and $\gamma = 4\pi\eta / \ln(2\xi/r)$ the drag coefficient, with η the solvent viscosity and r the filament radius.³⁰ Our computed value of $\tau_B \approx 0.54 \text{ s}$ is markedly close to our measured fast timescale, $\tau_1 \approx 0.56 \pm 0.06 \text{ s}$ before activity,³¹ and is similar to $\tau_1 \approx 0.42 \pm 0.16 \text{ s}$ measured after activity. As such, we attribute the fast relaxation timescale to filament bending, with actin contributing more so than the rigid microtubules within the composite. Note that while τ_1 values before and after activity are within error of each other, the average value after activity is $\sim 25\%$ lower and the standard deviation is $\sim 3x$ larger. The reduced average value could arise if the bending rigidity increased (due to motor-driven actin bundling) and/or if the effective filament radius increased (also due to bundling). The corresponding increase in variability could also arise from bundling as it would increase the structural heterogeneity of the composite.

To understand our slow relaxation timescales of $\tau_2 = 5.7 \pm 1.2$ s before activity and 5.0 ± 0.61 s after activity we note that our measured values are quite similar to the previously reported longest relaxation timescales of ~3-9 s for comparable actin-microtubule composites that lacked motors²⁹. As in this previous work, we attribute this timescale to a combination of reptation, whereby filaments diffused curvilinearly along their contour to relieve stress, and entanglement hopping, whereby filaments can periodically move transverse to their contours due to the temporary release of an entanglement with a neighboring filament.³¹

Finally, we evaluate the relative contributions $C_i/(C_1 + C_2)$ of each relaxation mechanism before and after activity (Fig 3C). We find that following activity the dominant relaxation mode shifts from the fast mode (bending) to the slow mode (facilitated reptation), with the fast mode contributing to 53% and 37% of the relaxation before and after, respectively. In other words, following motor-driven restructuring, reptation dominates the relaxation rather than the bending modes that dominate before activity. Motor activity may suppress the bending modes by causing filaments to bundle or cluster together, thereby becoming stiffer and less susceptible to thermal bending.²⁹

Our results of Figs 2 and 3 show that motor activity increases the elastic-like response and stiffness of the composites as well as the heterogeneity of the force response. As we suggest above, we hypothesize that these changes in the mechanical response of the composite are due to mesoscale restructuring of the composite from a homogeneous mesh of individual filaments to a more heterogeneous network of filament bundles and clusters. Specifically, previous studies have shown that bundling and crosslinking of entangled actin filaments causes increased crossover frequencies, higher elastic plateau moduli and more sustained elastic memory following relaxation.³²⁻³⁴ To test this hypothesis, we analyze images of the composite we acquire immediately before and after force measurements (Fig 4). Specifically, we label 10% of actin

monomers with AlexaFluor568 to enable visualization with 560 nm light that does not activate myosin (which requires 488 nm illumination).

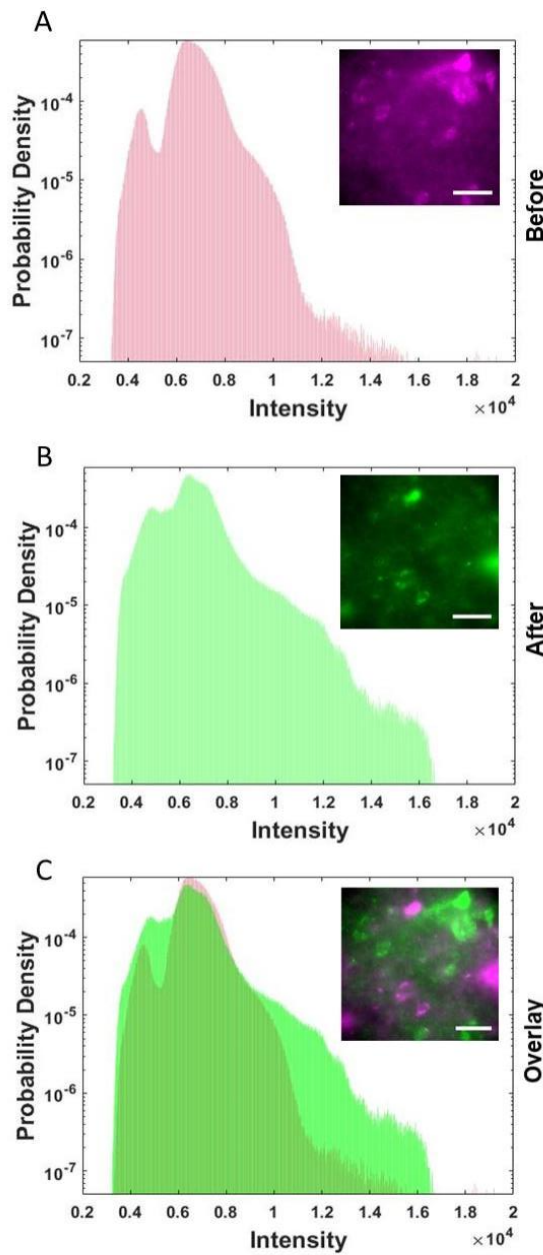


Figure 4. Myosin activity drives mesoscale motion and restructuring of actin-microtubule composites. Probability distributions of pixel intensity values from images collected before each nonlinear microrheology trial (A) before myosin II activity and (B) two hours after myosin II activation by 488 nm illumination for 10 s. (C) Overlay of histograms from (A) and (B). Insets: False-color fluorescence images of AlexaFluor568-labeled actin in the composite. Scale bars are 50 μ m. See SI for all images used in histograms. After myosin activity, local actin concentration is more likely to be below or above average than near average, a sign of increased heterogeneity.

Inspection of the overlay of these images (Fig 4C, inset) reveals large-scale network restructuring and movement of actin structures over the course of two hours. To quantify the observed network restructuring we examine the fluorescence intensity of images acquired before and after each measurement at different locations in the network separated by ~0.5 mm, using pixel intensity as a proxy for local actin density. Namely, a more clustered, heterogeneous network would result in a broader distribution, with a higher probability of high intensity values (high density clusters) and low intensity values (voids with little actin), whereas a more homogeneous mesh of filaments would have a narrower distribution of intermediate intensity values. The resulting histograms indeed show this expected trend (Fig 4), confirming that myosin II activity leads to composite contraction and clustering, and that the contracted bundles remain in such a configuration well after motor activity has ceased.

It is important to note that the structural and mechanical properties we report here are distinct from those expected for entangled actomyosin networks without microtubules. Namely, in actomyosin networks without crosslinkers, motor activity causes network rupturing and fluidization. Such activity would result in reduced elasticity and stiffness as well as unstable structure following activity. Here, the microtubules appear to act as a mechanical scaffold that reinforces the actin filaments, allowing myosin to contract actin into clusters without destroying connectivity, such that the composite can retain its mechanical integrity over extended periods of time and when subject to nonlinear forcing.²⁰

In summary, we couple optical tweezers microrheology with fluorescence microscopy to elucidate the effects of myosin II motor activity on the mechanical and structural properties of entangled composites of actin and microtubules. We show that motor activity increases the viscoelasticity and mechanical memory of the composite due to myosin-driven restructuring from

an entangled mesh of filaments into a network of dense filament bundles. This heterogeneous structure persists hours after cessation of motor activity, and leads to stronger resilience to nonlinear straining, increased stiffness, and suppressed filament bending. Our results provide valuable insight into the mechanics of active cytoskeletal systems, and how the interplay between motor activity, the composite nature of the cytoskeleton, and time-varying structure leads to the myriad of mechanical properties that cells exhibit. More generally, our techniques and results can be applied to a wide range of active matter systems currently under intense investigation.

Experimental Section

Many of the materials and methods are described in the main text and in the captions of Figs 1-4. More detailed descriptions of all materials and methods are included in the Supporting Information.

Supporting Information

Section 1. Materials and Methods

Figure S1. Fluorescence images of actin filaments in myosin-driven actin-microtubule composites show clustering and increased heterogeneity sustained hours after activation.

AUTHOR INFORMATION

Corresponding Author: Rae M Robertson-Anderson

Author Contributions. R.M.R.-A. conceived the project, guided the experiments, interpreted the data, and wrote the manuscript. J.Y.S designed and performed the experiments, analyzed and interpreted the data and wrote the manuscript. D.H.A. analyzed data and helped write the manuscript. K.P. helped guide experiments and analyzed and interpreted data. G.L. helped with materials preparation and data interpretation. M.J.R., M.D. and J.L.R. helped conceive the project and interpret data.

Acknowledgments. This research was funded by a William M. Keck Foundation Research Grant and a National Institute of General Medical Sciences Award (no. R15GM123420). J. Y. S. acknowledges startup support from the W. M. Keck Science Department of Claremont McKenna, Scripps, and Pitzer Colleges of The Claremont Colleges. The authors are grateful to Jonathan Garamella and Ryan McGorty for helpful discussions.

References

- (1) Burla, F.; Mulla, Y.; Vos, B.; Aufderhorst-Roberts, A.; Koenderink, G. From Mechanical Resilience to Active Material Properties in Biopolymer Networks. *Nat. Rev. Phys.* **2019**, 1. <https://doi.org/10.1038/s42254-019-0036-4>.
- (2) Fletcher, D. A.; Mullins, R. D. Cell Mechanics and the Cytoskeleton. *Nature* **2010**, 463 (7280), 485–492. <https://doi.org/10.1038/nature08908>.
- (3) Traffic control: regulation of kinesin motors | Nature Reviews Molecular Cell Biology <https://www.nature.com/articles/nrm2782> (accessed May 2, 2021).
- (4) Hartman, M. A.; Spudich, J. A. The Myosin Superfamily at a Glance. *J. Cell Sci.* **2012**, 125 (7), 1627–1632. <https://doi.org/10.1242/jcs.094300>.
- (5) Sanchez, T.; Chen, D. T. N.; DeCamp, S. J.; Heymann, M.; Dogic, Z. Spontaneous Motion in Hierarchically Assembled Active Matter. *Nature* **2012**, 491 (7424), 431–434. <https://doi.org/10.1038/nature11591>.
- (6) Needleman, D.; Dogic, Z. Active Matter at the Interface between Materials Science and Cell Biology. *Nat. Rev. Mater.* **2017**, 2 (9), 1–14. <https://doi.org/10.1038/natrevmats.2017.48>.

(7) Stossel, T. P. On the Crawling of Animal Cells. *Science* **1993**, *260* (5111), 1086–1094. <https://doi.org/10.1126/science.8493552>.

(8) Nonlinear mechanics of hybrid polymer networks that mimic the complex mechanical environment of cells | *Nature Communications* <https://www.nature.com/articles/ncomms15478> (accessed Apr 2, 2021).

(9) Bendix, P. M.; Koenderink, G. H.; Cuvelier, D.; Dogic, Z.; Koeleman, B. N.; Brieher, W. M.; Field, C. M.; Mahadevan, L.; Weitz, D. A. A Quantitative Analysis of Contractility in Active Cytoskeletal Protein Networks. *Biophys. J.* **2008**, *94* (8), 3126–3136. <https://doi.org/10.1529/biophysj.107.117960>.

(10) Koenderink, G. H.; Dogic, Z.; Nakamura, F.; Bendix, P. M.; MacKintosh, F. C.; Hartwig, J. H.; Stossel, T. P.; Weitz, D. A. An Active Biopolymer Network Controlled by Molecular Motors. *Proc. Natl. Acad. Sci.* **2009**, *106* (36), 15192–15197. <https://doi.org/10.1073/pnas.0903974106>.

(11) Storm, C.; Pastore, J. J.; MacKintosh, F. C.; Lubensky, T. C.; Janmey, P. A. Nonlinear Elasticity in Biological Gels. *Nature* **2005**, *435* (7039), 191–194. <https://doi.org/10.1038/nature03521>.

(12) Francis, M. L.; Ricketts, S. N.; Farhadi, L.; Rust, M. J.; Das, M.; Ross, J. L.; Robertson-Anderson, R. M. Non-Monotonic Dependence of Stiffness on Actin Crosslinking in Cytoskeleton Composites. *Soft Matter* **2019**, *15* (44), 9056–9065. <https://doi.org/10.1039/C9SM01550G>.

(13) Silva, M. S. e; Depken, M.; Stuhrmann, B.; Korsten, M.; MacKintosh, F. C.; Koenderink, G. H. Active Multistage Coarsening of Actin Networks Driven by Myosin Motors. *Proc. Natl. Acad. Sci.* **2011**, *108* (23), 9408–9413. <https://doi.org/10.1073/pnas.1016616108>.

(14) Murrell, M. P.; Gardel, M. L. F-Actin Buckling Coordinates Contractility and Severing in a Biomimetic Actomyosin Cortex. *Proc. Natl. Acad. Sci.* **2012**, *109* (51), 20820–20825. <https://doi.org/10.1073/pnas.1214753109>.

(15) Köster, D. V.; Husain, K.; Iljazi, E.; Bhat, A.; Bieling, P.; Mullins, R. D.; Rao, M.; Mayor, S. Actomyosin Dynamics Drive Local Membrane Component Organization in an in Vitro Active Composite Layer. *Proc. Natl. Acad. Sci.* **2016**, *113* (12), E1645–E1654. <https://doi.org/10.1073/pnas.1514030113>.

(16) Lenz, M. Geometrical Origins of Contractility in Disordered Actomyosin Networks. *Phys. Rev. X* **2014**, *4* (4), 041002. <https://doi.org/10.1103/PhysRevX.4.041002>.

(17) Wang, S.; Wolynes, P. G. Active Contractility in Actomyosin Networks. *Proc. Natl. Acad. Sci.* **2012**, *109* (17), 6446–6451. <https://doi.org/10.1073/pnas.1204205109>.

(18) Humphrey, D.; Duggan, C.; Saha, D.; Smith, D.; Käs, J. Active Fluidization of Polymer Networks through Molecular Motors. *Nature* **2002**, *416*, 413–416. <https://doi.org/10.1038/416413>.

(19) Smith, D.; Ziebert, F.; Humphrey, D.; Duggan, C.; Steinbeck, M.; Zimmermann, W.; Käs, J. Molecular Motor-Induced Instabilities and Cross Linkers Determine Biopolymer Organization. *Biophys. J.* **2007**, *93* (12), 4445–4452. <https://doi.org/10.1529/biophysj.106.095919>.

(20) Lee, G.; Leech, G.; Rust, M. J.; Das, M.; McGorty, R. J.; Ross, J. L.; Robertson-Anderson, R. M. Myosin-Driven Actin-Microtubule Networks Exhibit Self-Organized Contractile Dynamics. *Sci. Adv.* **2021**, *7* (6), eabe4334. <https://doi.org/10.1126/sciadv.abe4334>.

(21) Squires, T. M. Nonlinear Microrheology: Bulk Stresses versus Direct Interactions. *Langmuir* **2008**, *24* (4), 1147–1159. <https://doi.org/10.1021/la7023692>.

(22) Nishizawa, K.; Bremerich, M.; Ayade, H.; Schmidt, C. F.; Ariga, T.; Mizuno, D. Feedback-Tracking Microrheology in Living Cells. *Sci. Adv.* **2017**, *3* (9), e1700318. <https://doi.org/10.1126/sciadv.1700318>.

(23) Tassieri, M.; Evans, R. M. L.; Warren, R. L.; Bailey, N. J.; Cooper, J. M. Microrheology with Optical Tweezers: Data Analysis. *New J. Phys.* **2012**, *14* (11), 115032. <https://doi.org/10.1088/1367-2630/14/11/115032>.

(24) Mason, T. G. Estimating the Viscoelastic Moduli of Complex Fluids Using the Generalized Stokes–Einstein Equation. *Rheol. Acta* **2000**, *39* (4), 371–378. <https://doi.org/10.1007/s003970000094>.

(25) Peddireddy, K. R.; Lee, M.; Schroeder, C. M.; Robertson-Anderson, R. M. Viscoelastic Properties of Ring-Linear DNA Blends Exhibit Nonmonotonic Dependence on Blend Composition. *Phys. Rev. Res.* **2020**, *2* (2), 023213. <https://doi.org/10.1103/PhysRevResearch.2.023213>.

(26) Nonequilibrium Mechanics of Active Cytoskeletal Networks | Science <https://science.sciencemag.org/content/315/5810/370.full> (accessed Apr 25, 2021).

(27) MacKintosh, F. C.; Levine, A. J. Nonequilibrium Mechanics and Dynamics of Motor-Activated Gels. *Phys. Rev. Lett.* **2008**, *100* (1), 018104. <https://doi.org/10.1103/PhysRevLett.100.018104>.

(28) Doi, M.; Edwards, S. F. *The Theory of Polymer Dynamics*; Clarendon Press: Oxford, 1988.

(29) Ricketts, S. N.; Francis, M. L.; Farhadi, L.; Rust, M. J.; Das, M.; Ross, J. L.; Robertson-Anderson, R. M. Varying Crosslinking Motifs Drive the Mesoscale Mechanics of Actin-Microtubule Composites. *Sci. Rep.* **2019**, *9* (1), 12831. <https://doi.org/10.1038/s41598-019-49236-4>.

(30) Flexural Rigidity of Microtubules and Actin Filaments Measured from Thermal Fluctuations in Shape. *J. Cell Biol.* **1993**, *120* (4), 923–934.

(31) Ricketts, S. N.; Ross, J. L.; Robertson-Anderson, R. M. Co-Entangled Actin-Microtubule Composites Exhibit Tunable Stiffness and Power-Law Stress Relaxation. *Biophys. J.* **2018**, *115* (6), 1055–1067. <https://doi.org/10.1016/j.bpj.2018.08.010>.

(32) Shin, J. H.; Gardel, M. L.; Mahadevan, L.; Matsudaira, P.; Weitz, D. A. Relating Microstructure to Rheology of a Bundled and Cross-Linked F-Actin Network in Vitro. *Proc. Natl. Acad. Sci. U. S. A.* **2004**, *101* (26), 9636–9641. <https://doi.org/10.1073/pnas.0308733101>.

(33) Lee, H.; Ferrer, J. M.; Nakamura, F.; Lang, M. J.; Kamm, R. D. Passive and Active Microrheology for Cross-Linked F-Actin Networks in Vitro. *Acta Biomater.* **2010**, *6* (4), 1207–1218. <https://doi.org/10.1016/j.actbio.2009.10.044>.

(34) Gurmessa, B.; Francis, M.; Rust, M. J.; Das, M.; Ross, J. L.; Robertson-Anderson, R. M. Counterion Crossbridges Enable Robust Multiscale Elasticity in Actin Networks. *Phys. Rev. Res.* **2019**, *1* (1), 013016. <https://doi.org/10.1103/PhysRevResearch.1.013016>.